Magnetic field regulating the graphite anode for excellent lithium-ion batteries performance

Li Zhang [a, b*], Mingyang Zeng [a, b], Dandan Wu [a, b], Xingbin Yan [b, c, d *]

[a] Department of Physics, School of Science, Lanzhou University of Technology, 287 Langongping Avenue, Lanzhou, Gansu, 730050, P. R. China.

[b] Laboratory of Clean Energy Chemistry and Materials, State Key Laboratory of Solid Lubrication, Lanzhou Institute of Chemical Physics, Chinese Academy of Sciences, 18 Tianshui Avenue, Lanzhou, Gansu, 730000, P. R. China.

[c] Center of Materials Science and Optoelectronics Engineering, University of Chinese Academy of Sciences, 19 Yuquan Avenue, Beijing, 100080, P. R. China.

[d] Dalian National Laboratory for Clean Energy, Dalian Institute of Chemical Physics, Chinese Academy of Sciences, 457 Zhongshan Avenue, Dalian, Liaoning, 116000, P. R. China.

[*] Corresponding Authors.

E-mail: zhangli@lut.cn (L. zhang) and xbyan@licp.cas.cn (X. B. Yan).

Total Number of Pages: 17

Total Number of Figures: 17

Total Number of Tables: 2

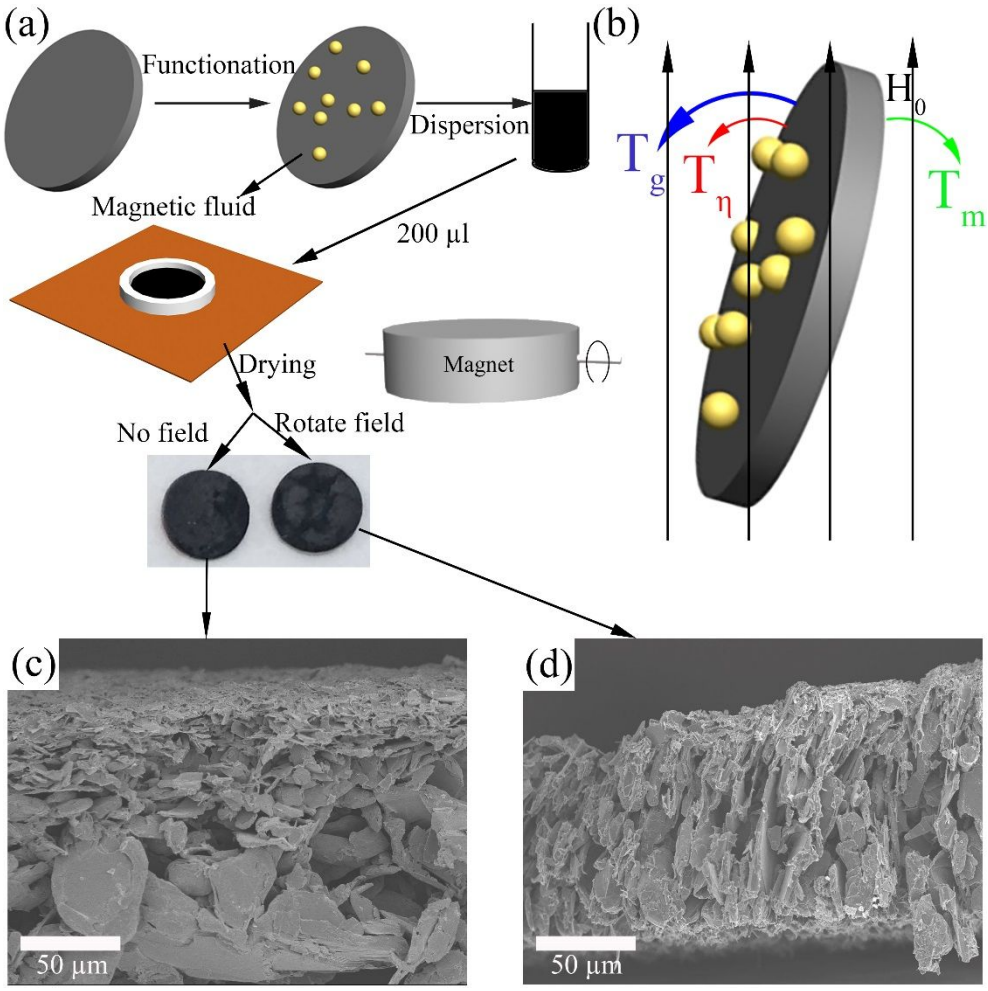

Figure S1. (a) Detailed process for preparing graphite negative electrode. (b) Schematic of graphite flakes in the process of alignment with an out-of-plane magnetic field H_0. Fe_3O_4 nanoparticles adsorbed on the flakes surface is expressed by yellow balls. (c) and (d) Cross-sectional SEM images of the reference electrode and aligned electrodes, respectively.

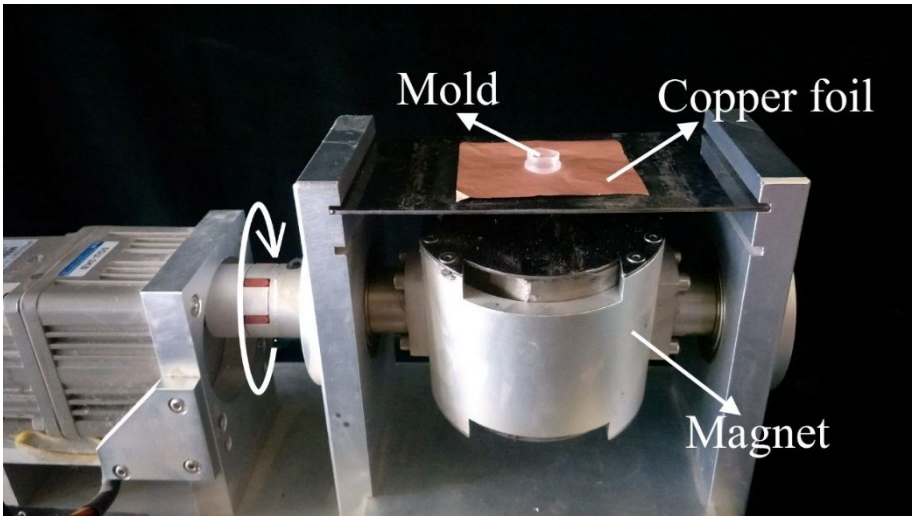

Figure S2. The equipment used for casting the graphite electrode following magnetic alignment flakes.

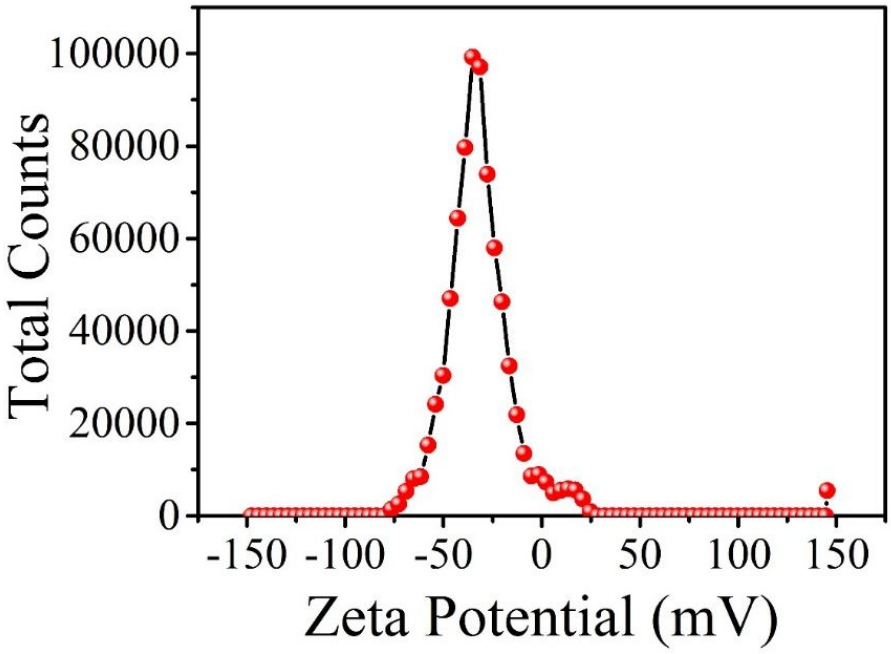

Figure S3. Zeta potential of the graphite flakes in water at pH=7.

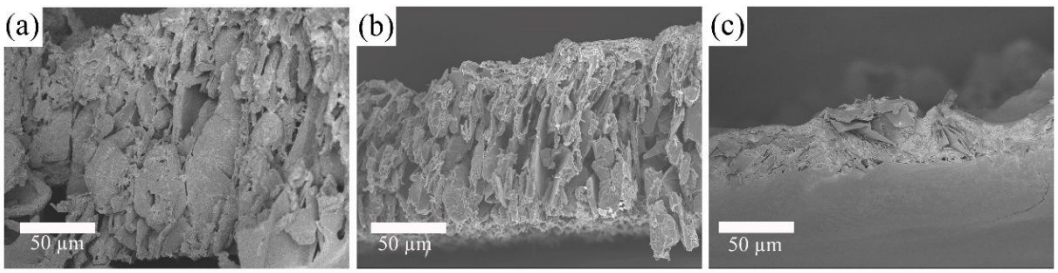

Figure S4. (a)-(c) Cross-sectional SEM images of the graphite electrodes obtained at the suspension concentrations of 0.1 g ml^{-1}, 0.05 g ml^{-1} and 0.025 g ml^{-1}, respectively.

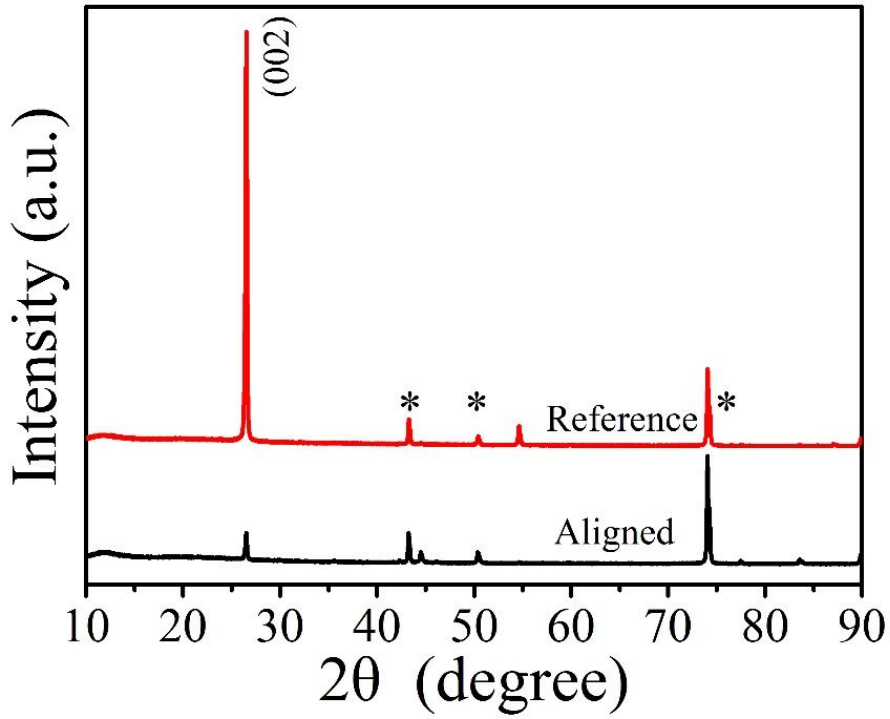

Figure S5. XRD images of aligned graphite electrode and reference electrode.

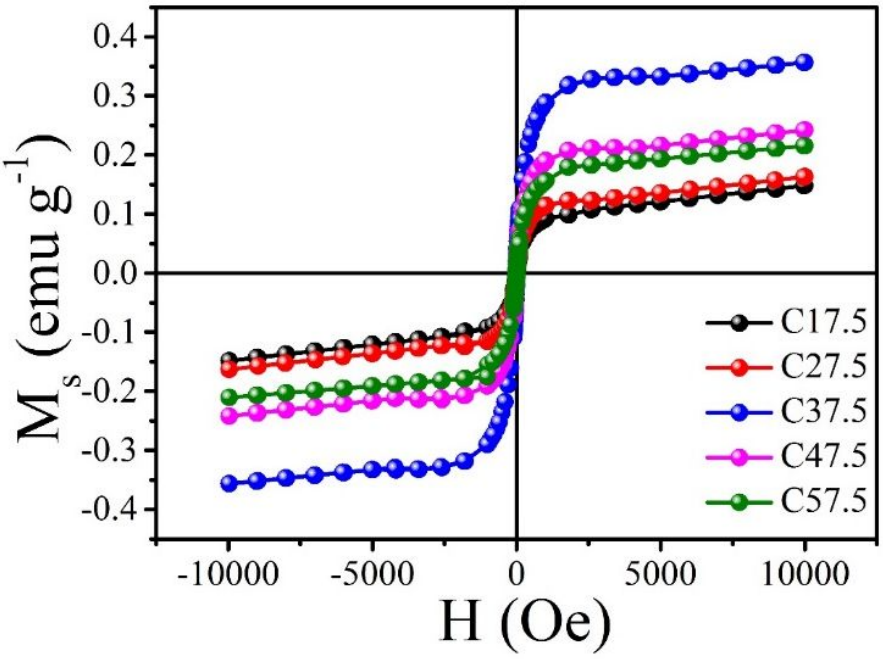

Figure S6. Magnetic hysteresis loops of functional graphite which prepared at different concentration of ferrofluid.

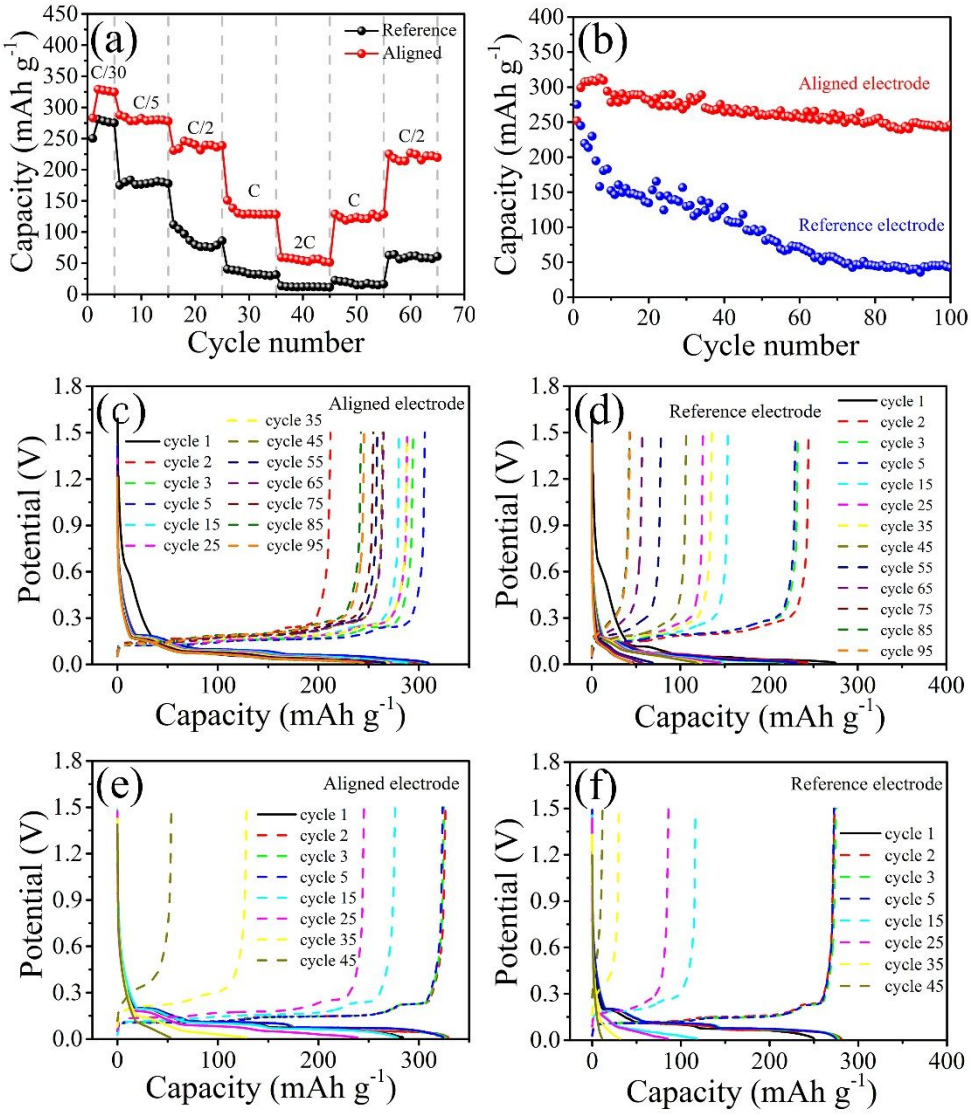

Figure S7. (a) Rate capabilities and (b) Evolution of the specific charge at rate of C/30 for aligned and reference electrodes, respectively. Galvanostatic charge-discharge profiles of (c) aligned and (d) reference electrodes at a low current rate of C/30 between 0 and 1.5 V versus Li^+/Li. Galvanostatic charge-discharge profiles of (e) aligned and (f) reference electrodes corresponding to first five cycles at rate of C/30, 15^{th} cycle at the rate of C/10, 25^{th} cycle at the rate of C/2, 35^{th} cycle at the rate of C and 45^{th} cycle at the rate of 2C, respectively.

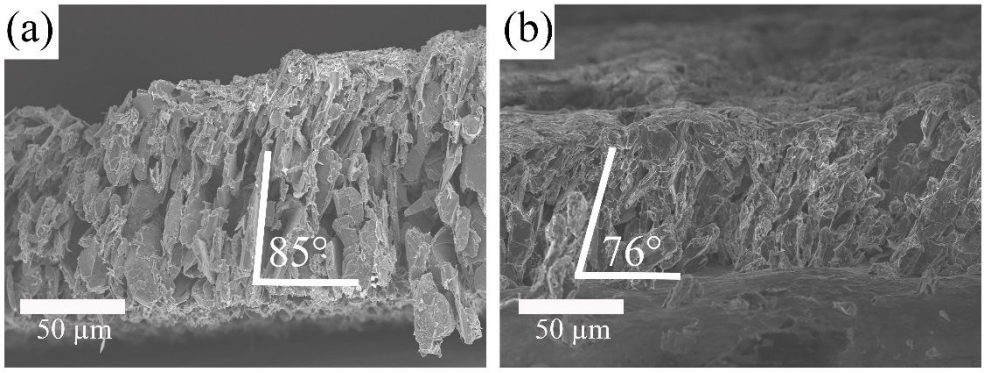

Figure S8. Cross-sectional SEM images of aligned electrode (c) before and (d) after cycling at rate of 1C.

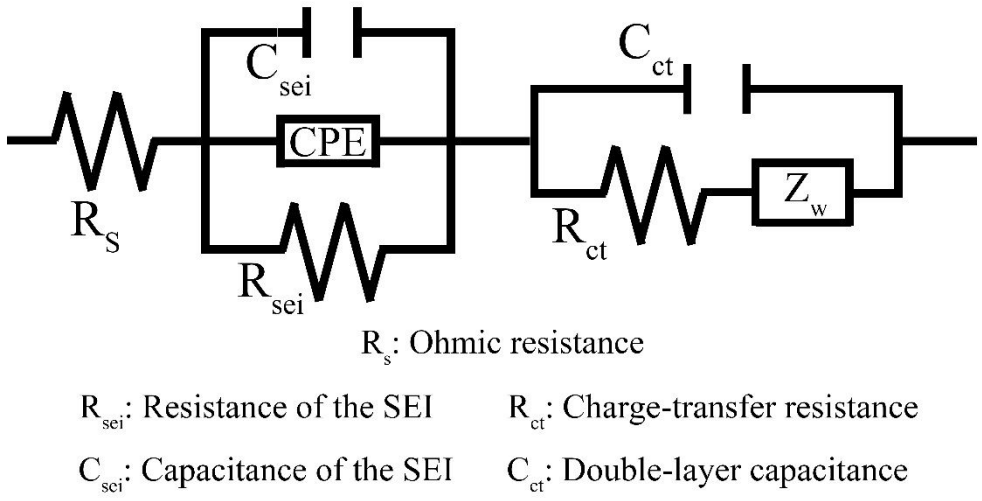

Figure S9. Modeled equivalent circuit of EIS.

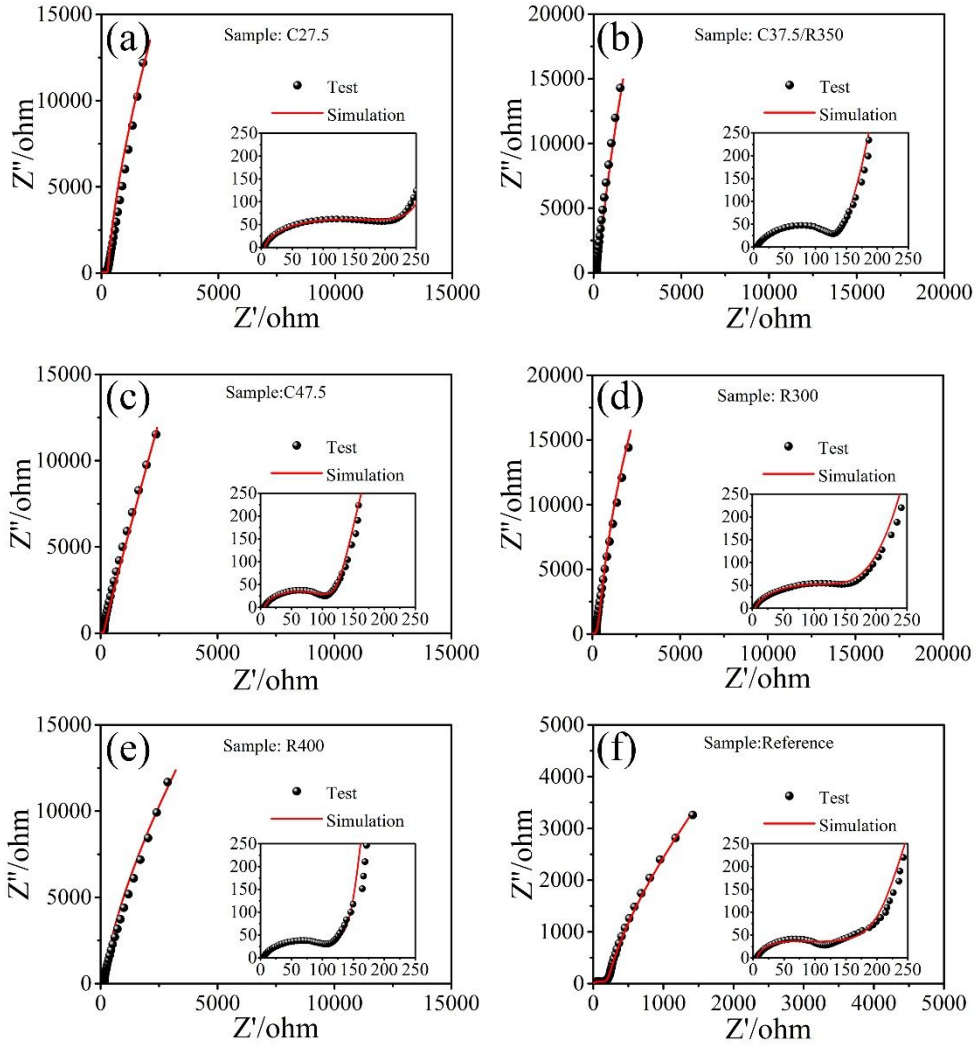

Figure S10. Experimental and simulated EIS spectra with the equivalent circuit of electrodes (a) C27.5, (b) C37.5/R350, (c) C47.5, (d) R300, (e) R400, (f) reference (high-frequency region Nyquist plots as an inset).

Table S1. Electrode resistance obtained from equivalent circuit fitting of experimental data.

Sample	Angle (°)	R_s (Ω)	R_{sei} (Ω)	R_{ct} (Ω)	Z_w (10^{-5})
C27.5	71	6.736	309.8	2.897	5.407
C37.5/R350	85	6.599	168	1.912	2.694
C47.5	72	6.488	138.1	2.431	7.509
R400	60	6.502	166.3	5.883	9.621
R300	74	6.987	291.4	2.112	4.165
Reference	4	7.021	302.1	6.661	54.4

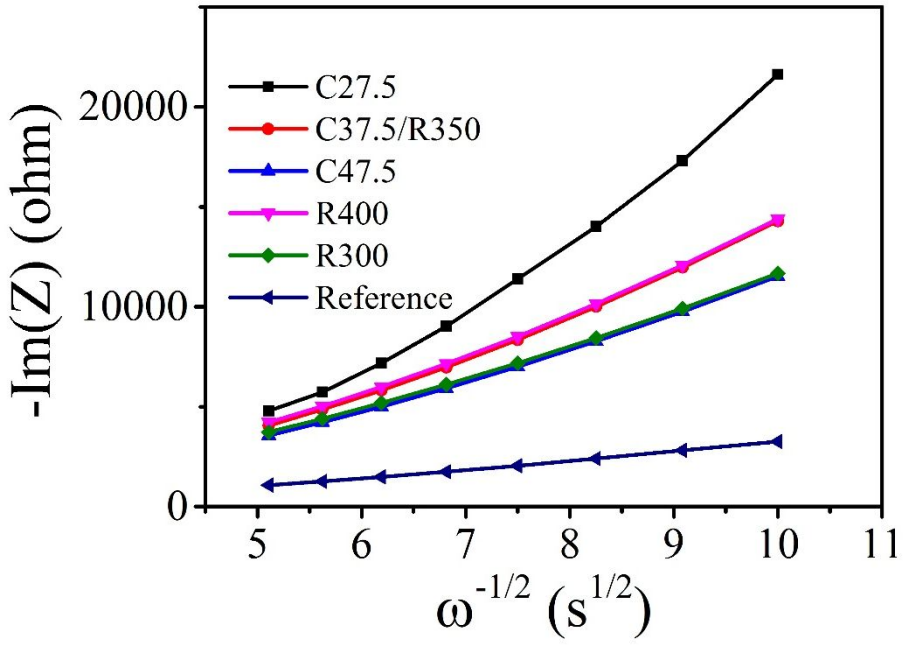

Figure S11. The -Im (Z) as a function of $\omega^{-1/2}$ in low frequency region for C27.5, C37.5/R350, C47.5, R300, R400 and reference electrodes.

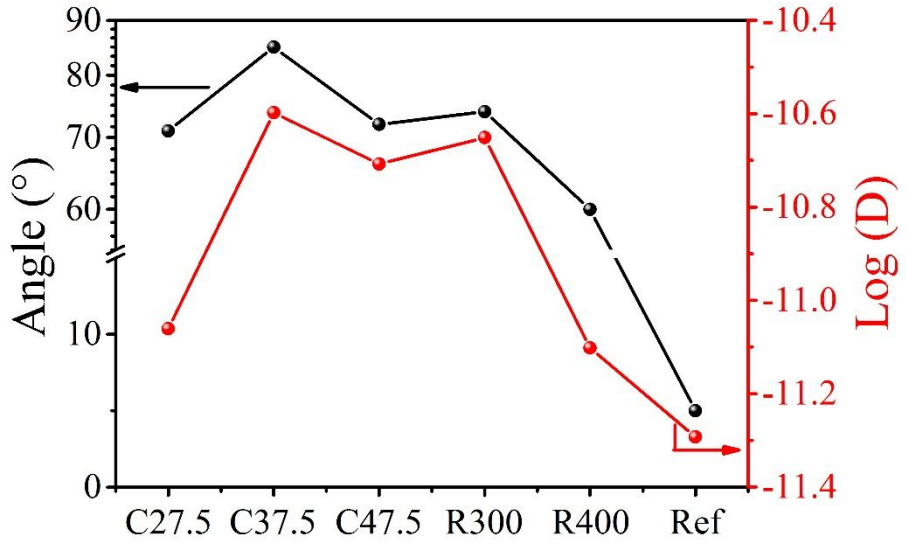

Figure S12. The relationship between diffusion coefficient of Li^+ and the alignment degree of C27.5, C37.5/R350, C47.5, R300, R400 and reference electrodes.

Table S2. Comparison between the electrochemical performance of the aligned structure electrodes previously reported and that of our electrodes.

Material	Current density	Capacity retention	Thickness (μm)	References
Si/CNT	1.3C-15C	25.7%	≈10	Ref.20
ZnO/graphene	80-6400 mA g^{-1}	24.8%	≈1	Ref.37
CNT/graphene paper	0.1C-10C	17.9%	≈40	Ref.21
Graphite	C/30-2C	14.7%	≈200	Ref.31
graphene/GeO_x	0.5C-15C	56%	3-10	Ref.38
Ge/CNT	0.5C-10C	60%	≈0.93	Ref.22
Graphite	C/30-2C	18.5%	≈160	This work

Calculation method

The critical angle velocity can be obtained by the following formula:

$$\omega_c = \frac{\mu_0 \chi_{ps}^2 H_0^2}{18\left(f/f_0\right)\eta(\chi_{ps}+1)}\left[\frac{(a+d)(b+d)^2}{ab^2}-1\right] \quad \text{(S1)}$$

where χ_{ps} represents the susceptibility of functionalized graphite that is equal to the ratio of the special magnetization M_s to magnetic field intensity H, where M_s is observed by the magnetic hysteresis loops (as shown in Fig. S6). By calculation, χ_{ps} of functionalized graphite which is prepared with the ferrofluid concentration of 17.5, 27.5, 37.5, 47.5 and 57.5 μl g^{-1} are 0.573, 0.631, 1.382, 0.937 and 0.836, respectively. The value of H_0 is 2379 Oe measured by a digital Gauss meter. The viscosity η of suspension measured with capillaries is 18.3 mPa·s. d represents the diameter of Fe_3O_4 nanoparticle which is about 12 nm.

In this experiment, two types of graphite flakes with different particle sizes are used. To explore the effect on the alignment, keeping other experimental parameters (the rotating speed of 350 r min^{-1} and the ferrofluid concentration of 37.5 μl g^{-1}), we prepare the electrodes with different mass ratio of large graphite flakes to small graphite flakes, which are 1:0, 4:1, 1:1, 1:4 and 0:1, respectively. Fig. S13 shows the cross-sectional SEM images of electrodes, which demonstrate the angles of 73°, 85°, 68°, 58° and 45°, respectively. It is observed that all the small flakes (0:1) or more small flakes (1:4) are not conducive to the alignment of the graphite while the ratio of 4:1 is beneficial to obtain the alignment with higher angle. It means that large graphite flakes as host materials plays a sustaining role and the small graphite plays a correction role during the alignment of electrodes. Therefore, the ratio of 4:1 is fixed in the following study. And the value of a and b is identified as half the thickness and half the diameter of large graphite flakes because the mass of small flakes is negligible relative to large flakes, which a is 4.1μm and b is 22 μm:

$$\frac{f}{f_0} = \frac{4}{3}\frac{1-p^2}{(2-p^2 aS)} \tag{S2}$$

Where, p = b/a

$$S = \frac{(2/a)}{(p^2-1)^{1/2}tan\left[(p^2-1)^{1/2}\right]} \tag{S3}$$

The value of f/f_0 is calculated to be 0.31841.

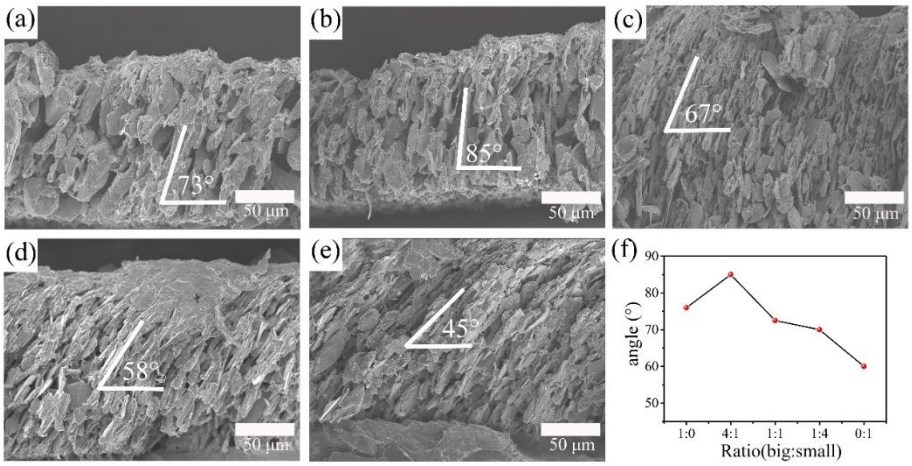

Figure S13. Cross-sectional SEM images of graphite negative electrodes prepared with the ratio of large graphite to small graphite are (a) 1:0, (b) 4:1, (c) 1:1, (d) 1:4, (e) 0:1, respectively. (f) Evolution of the angle as a function of the ratio of large graphite to small graphite.

Electrode Tabletting

From EIS results, it is observed that the aligned electrodes exhibit relatively higher charge transfer impedance compared with that of reference electrode. This is mainly due to the poor contact between the aligned flakes and current collector. Generally, tableting is the necessary step for preparing the conventional electrode, which can increase the contact area between the electrode materials and the current collectors and reduce the charge transfer impedance. However, the step of tableting is absent in the process of preparing the aligned electrode. Therefore, we attempt to tablet the aligned electrodes and explore the effect of tabletting on the aligned structure and performance of electrodes. Here, C37.5 as the typical electrode, is tableted under the pressure of 1000N, 1500N, 2000N, 2500N, 3000N, 3500N and 4000N, respectively. Fig. S14 (a)-(h) shows cross-section SEM images of electrodes tabletting at different pressures. It is obviously that tableting has some effect

on the degree of alignment, although the alignment remains. The angles are 85°, 68°, 72°, 78°, 74°, 69°, 63° and 50° corresponding to the pressure of 0N, 1000N, 1500N, 2000N, 2500N, 3000N, 3500N and 4000N, respectively, which are lower than that of C37.5. The results are further confirmed by XRD images (as seen in Fig. S14i). It is shown that angles tend to increase first and then decrease, which can be explained by force analysis. As shown in the Fig. S16, the pressure (expressed with "F") from tabletting is perpendicular to the current collector which can be decomposed in two directions (the component force F_1 perpendicular to graphite flakes and the component force F_2 parallel to graphite flakes). The force F_1 and F_2 are expressed in the terms of $F\cos\theta$ and $F\sin\theta$, respectively. The force F_2 can not only improve the order degree of electrode in the extrusion process, but also make the graphite electrode becoming more compact, while the force F_1 can drive graphite flakes progressively paralleling to current collectors. These two forces compete with each other. Exerting a relatively small F on electrode, force F_2 is much larger than force F_1, so that the effect of force F_1 on electrodes is negligible and force F_2 can improve the order degree of the electrodes. When gradually increasing F, force F_1 act on the electrodes to further destroy the order degree.

Considering that the 1000N is a minimum force, we assemble the half-cell and measure the electrochemical performance. Fig. S15 shows the rate performance of tableted, non-tableted and reference electrodes at different rates. The specific capacity of tableted electrode is obviously higher than that of non-tableted electrode when the rate is less than C/5. While the rate exceeds C/5, the specific capacity of tableted electrode rapidly decreases compared with non-tableted electrode because of the ordering damage. Surprisingly, the specific capacity of tableted electrode is still higher than that of reference electrode especially at high rate, which improve the rate performance

of electrode. Moreover, Fig. S15d displays that the charge-transfer resistance becomes smaller after tableting, which indicating tabletting can effectively improve the charge transfer in electrodes. In the follow work, we will further improve the tableting process to enhance the rate performance of LIBs.

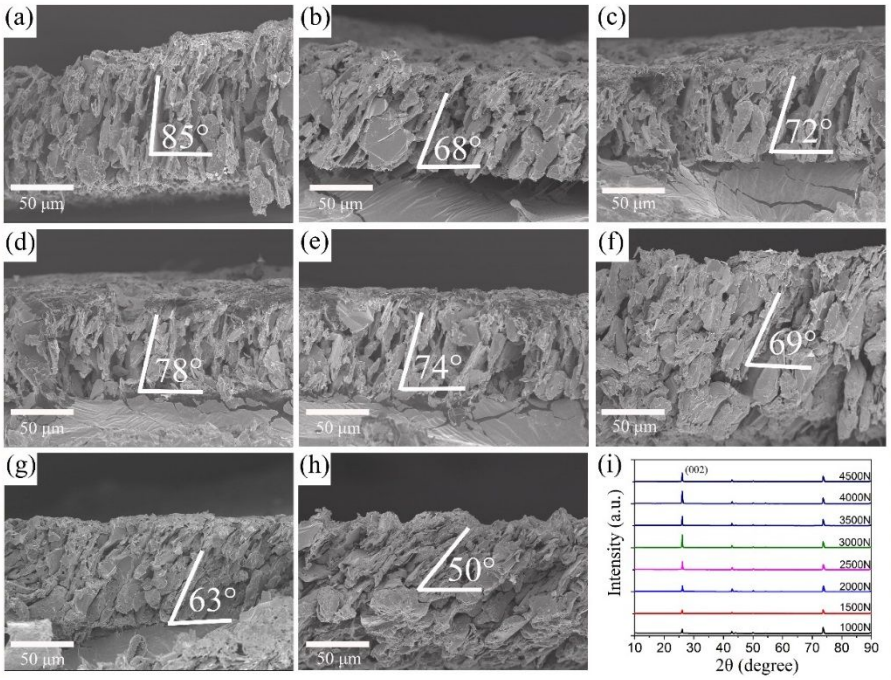

Figure S14. (a)-(h) Cross-sectional SEM images of electrodes tableted at different pressure of 0 N, 1000 N, 1500 N, 2000 N, 2500 N, 3000 N, 3500 N and 4000 N, respectively. (i) XRD images of electrodes tableted at different pressure.

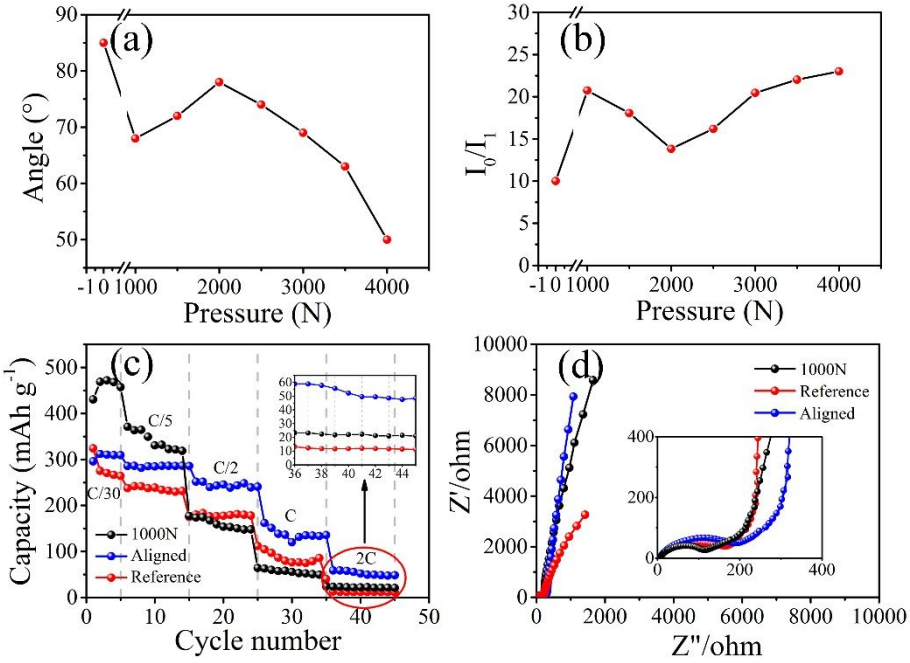

Figure S15. (a) The relationship between the angle of graphite electrodes and tableting pressure. (b) Tableting pressure dependence of relative intensity ratio of 26° peak to 56° peak. (c) Rate performance of electrodes before and after tabletting at 1000N reference electrode. (d) EIS images of electrodes before and after tabletting at 1000N and reference electrode.

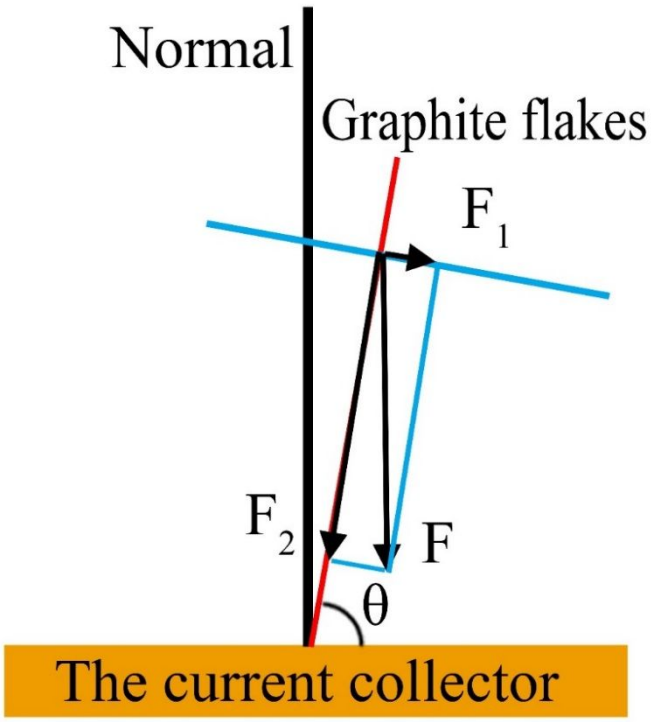

Figure S16. The force analysis of graphite flakes in the process of tabletting.

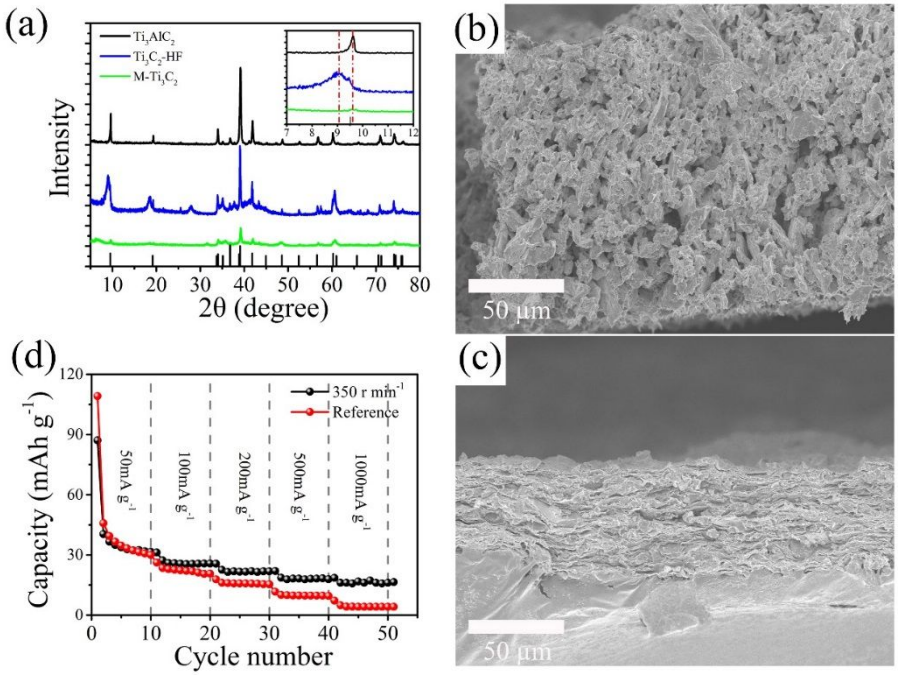

Figure S17. Magnetic arrangement for Ti_3C_2 electrodes. (a) XRD patterns of Ti_3AlC_2, multilayer Ti_3C_2 and few-layer Ti_3C_2. (b) and (c) Cross-sectional SEM images of the aligned and unaligned electrodes, respectively. (d) The rate capacity of unaligned and aligned Ti_3C_2 electrodes.

Multilayer Ti_3C_2 is prepared by exfoliating the Al element from the Ti_3AlC_2 in 40 % HF solution at room temperature for 24 h. The few-layer Ti_3C_2 is prepared via a mechanical-milling method with a planetary ball-mill apparatus. The structure and phase characteristics of Ti_3AlC_2, Ti_3C_2-HF and M- Ti_3C_2 are determined by XRD as shown in the Fig. S17a. According to the formula (1), we can get ω_c = 33 rad s^{-1}, which corresponding rotating speed of 315 r min^{-1}. In the parameters, a and b are 0.5 μm and 2 μm, respectively. χ_{ps} is 0.937 which corresponding ferrofluid concentration is 37.5 μl g^{-1}. η is 18.3 mPa·s. Therefore, we prepared the Ti_3C_2 (MXene) electrode at rotating speed of 350 r min^{-1}. As shown in the Fig. S17c, in the unaligned electrode, Ti_3C_2 flakes are almost parallel to the current collector and densely packed. However, in the aligned electrode, Ti_3C_2 flakes are almost vertically to the current collector (as shown in the Fig. S17b). In order to investigate the electrochemical performance of Ti_3C_2 electrodes prepared magnetic field, the rate performance is tested in a half-cell configuration. As shown in the Fig. S17d, the specific capacity of aligned electrode is 17.2 mAh g^{-1} which is 4.2 times the specific capacity of unaligned electrode which is 4.2 mAh g^{-1}. The specific capacity can be further improved by optimizing the rotating speed in further work.